Development of One-Dimensional Band Structure in Artificial Gold Chains

N. Nilius, T. M. Wallis,* W. Ho†

The ability of a scanning tunneling microscope to manipulate single atoms is used to build well-defined gold chains on NiAl(110). The electronic properties of the one-dimensional chains are dominated by an unoccupied electron band, gradually developing from a single atomic orbital present in a gold atom. Spatially resolved conductance measurements along a 20-atom chain provide the dispersion relation, effective mass, and density of states of the free electron–like band. These experiments demonstrate a strategy for probing the interrelation between geometric structure, elemental composition, and electronic properties in metallic nanostructures.

The formation of a bulk crystal from single metal atoms is accompanied by a dramatic change in physical and chemical properties. Small metal aggregates show strong catalytic activity, unknown for bulk structures with identical chemical composition (*1*, *2*). The distinct absorption behavior of metal clusters provides a basis for various optical applications (*3*, *4*). The characteristic properties of matter in the atom-to-bulk transition range partly result from a strong size dependence of the electronic structure. The discrete energy levels of isolated atoms split and broaden to electron bands in larger aggregates. The band structure determines the propagation and mobility of electrons inside the crystal. In principle, control over the size-dependent electronic structure allows an adjustment of intrinsic material properties to the demands of a wide range of applications.

Whereas band-structure engineering has seen remarkable success in semiconductor technology, the investigation and tailoring of electronic properties is only just beginning for nanosized metal structures. The high electron density and efficient screening in metals make the critical length scale for the atom-to-bulk-transition considerably smaller than for semiconductors. Gradual development of metallic behavior has been observed for ultrasmall clusters, either in the gas phase or on surfaces (*5*, *6*). The transition is characterized by the closure of gaps in the electronic states and the development of collective electronic excitations. However, incomplete knowledge of their geometric structure complicates the analyses of intrinsic cluster properties.

Starting from the opposite side of the transition range, the bulk electronic structure can be gradually confined in low-dimensional systems. Two-dimensional (2D) states are formed on metal surfaces (*7*–*9*). Step edges and linear adsorbate configurations cause the development of one-dimensional (1D) electron bands (*10*–*12*). Low-dimensional electron systems exhibit properties that are fundamentally different from those of bulk solids, such as strong electron-electron correlations or a distinct screening behavior (*13*). Preparation and analysis of well-defined nanosized structures remain the biggest challenge for studying the transition from atomic to bulklike electronic behavior. The experiments described here take advantage of the unique ability of a scanning tunneling microscope (STM) to manipulate single atoms on metal surfaces (*14*). Linear Au chains were built on NiAl(110), adding one atom at a time. Their electronic properties were derived from scanning tunneling spectroscopy (STS) and revealed the evolution of a 1D band structure from a single atomic orbital.

The experiments were carried out in an ultrahigh-vacuum STM operated at 12 K (*15*). The NiAl(110) single crystal was prepared by alternating cycles of Ne^+ sputtering and annealing to 1300 K. Single Au atoms, deposited on NiAl(110) at 12 K, appear as protrusions in topographic STM images. The preferential adsorption site is identified as the bridge position on Ni troughs, which alternate with protruding Al rows on the alloy surface (Fig. 1A). At low tunnel resistance (V/I < 150 kilohm), a single Au atom can be moved across the surface, jumping from one to the next adsorption site as it follows the trajectory of the tip ("pulling mode") (*16*). Increasing the resistance above 1 gigohm provides stable conditions for imaging and spectroscopy of surface structures. The controlled manipulation of Au atoms is used to build 1D chains along the Ni troughs, which serve as a natural template (Fig. 1). The atom-atom separation is given by the distance between adjacent Ni bridge sites (2.89 Å) and matches the nearest neighbor distance in bulk Au (2.88 Å). For every atom added to the structure, the measured chain length increased by ~3 Å. Individual Au atoms in a chain are indistinguishable in STM images, indicating a strong overlap of their atomic wave functions.

The electronic properties of the Au chains were determined by STS, which detects the derivative of the tunneling current as a function of sample bias with open feedback loop. The tunneling conductance (dI/dV) gives a measure of the local density of states (DOS) available for tunneling electrons. Probing the empty states of NiAl(110) at positive sample bias reveals a smooth increase in conductivity, reflecting the DOS of the NiAl sp-band (Fig. 2). In contrast, STS of a Au monomer is dominated by a Gaussian-shaped conductivity peak centered at 1.95 V. The resonance is reproduced with different tips and shows a spatial extension comparable to the size of the atom in topographic images. The enhanced conductance is attributed to resonant tunneling into an empty state in the Au atom. Its localization outside the atom in the tip-

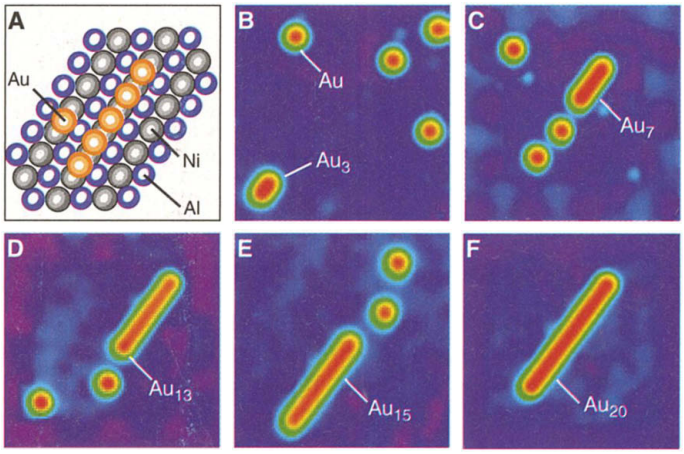

Fig. 1. (**A**) Structure model of a Au_5 chain and a Au atom on NiAl(110). (**B** to **F**) STM topographic images showing intermediate stages of building a Au_{20} chain. Single Au atoms were manipulated with the STM tip and attached on both sides to the chain (image sizes 95 Å by 95 Å, V_{sample} = 2.1 V, I = 1 nA).

Department of Physics and Astronomy and Department of Chemistry, University of California, Irvine, CA 92697–4575, USA.

*On leave of absence from Department of Physics, Cornell University, Ithaca, NY 14853–2501, USA.
†To whom correspondence should be addressed. E-mail: wilsonho@uci.edu

sample junction points to a slowly decaying state with sp character, which most likely arises from the hybridization of atomic Au orbitals and NiAl states.

Moving a second Au atom into a next neighbor position on the Ni row leads to a dramatic change of the electronic properties. The single resonance at 1.95 V splits into a doublet with peaks at 1.50 and 2.25 V, indicating strong coupling between the two atoms (Fig. 2). The energy splitting appears to be analogous to the well-known example of two hydrogen 1s states forming a bonding and an antibonding level in a H_2 molecule. The formation of a linear Au trimer shifts the low-energy peak to 1.1 eV and the high-energy peak to 2.6 eV. A third peak emerges at 1.8 V, as predicted in molecular orbital theory from the overlap of three initial Au orbitals. The relative intensity of the resonances changes with tip position over the trimer. To allow comparison, all spectra in Fig. 2 are taken in the center of Au chains. Individual conductivity resonances become indistinguishable for chains containing more than three atoms, because of the overlap between neighboring peaks and the finite peak width of 0.35 V. However, adding more atoms to the chain causes a continuous downshift of the lowest energy peak from 0.95 eV for Au_4 to 0.75 eV for a 20-atom chain (Fig. 2). Reproducing the experiment with different STM tips gives an identical relation between peak energy and chain length (*17*).

Mapping the conductivity at different positions along a chain reveals a characteristic intensity pattern, as demonstrated with a series of *dI/dV* spectra taken on a Au_{20} chain (Fig. 3A). The conductance in the center is dominated by low-energy peaks around 0.75 eV, fading out as the tip moves outward. A peak around 2.4 V emerges on both ends of the chain. Similar results were observed for shorter Au chains. The conductivity modulations along the chain are more obvious in constant energy cuts (Fig. 3C) made through the spectra of Fig. 3A. Because of the well-defined geometry of Au chains on NiAl(110), a 1D quantum well with infinite walls can be used to analyze the observed *dI/dV* patterns. The model is justified by the presence of a pseudo band gap in the DOS of NiAl(110) located above the Fermi level, which reduces the influence of substrate electronic states (*18*). To account for a finite barrier height, the absolute length of the well (L) is treated as an adjustable parameter. For Au_{20}, L varies from 59 to 62 Å with increasing energy, in agreement with the chain length determined from topographic STM images. The observed conductivity pattern results from a combination of two effects. (i) The electron transport through the 1D quantum well is limited to a finite number of discrete electronic levels E_n, given by the length and the depth of the well. The measured *dI/dV* signal is high, when the sample bias matches one of the energy levels. (ii) Along the chain axis, the conductivity is determined by the squared wave function $\phi_n(k)^2$, describing the probability density of electrons in the corresponding state E_n. For a 1D quantum well, the $\phi_n(k)$ are sinusoidals with discrete wave vectors $k = \pm\pi n/L$ and the quantum number of states n (*19*). Conductivity minima along the chain are expected at nodes of the corresponding wave function. Because of the finite width of the energy levels, more than one state contributes to the differential conductance at a selected sample bias, and *dI/dV* patterns are superpositions of several wave functions. An energy-dependent coefficient c_n accounts for the varying weight of individual wave functions at different sample voltages (*20*).

The *dI/dV* pattern observed at low sample bias can be fitted with a superposition of the wave functions ϕ_1 to ϕ_4. With increasing bias, the contribution of slowly varying wave functions vanishes, and states with higher wave vectors gradually gain weight. Intensity patterns around 1.5 V are reproduced with nonzero values for c_5 to c_7, and two coefficients (c_{11},c_{12}) are sufficient around 2.5 V (Fig. 3C). The fitting procedure reveals a Gaussian-shaped energy dependence for the coefficients c_n, demonstrating the varying contribution of the corresponding wave functions to the *dI/dV* pattern at a specific sample bias (Fig. 4A). The maximum value for every c_n defines the energy position of an electronic state E_n in the quantum well and relates it to the wave vector k of the corresponding wave function. A plot of energy–wave vector pairs yields the dispersion relation for electronic states in the Au_{20} chain (Fig. 4B). The points $E_n(k)$ are aligned on a parabolic curve, as expected for a 1D free electron–like band. A fit to the theoretical dispersion relation

$$E(k) = E_o + (\hbar^2/2m_{eff})k^2 \qquad (1)$$

gives a band onset E_o of 0.68 eV and an effective mass (m_{eff}) of 0.5 times the free-electron mass (m_e) (*19*).

Assembling 20 Au atoms to a linear chain has resulted in the formation of a 1D electron band from a single Au atomic orbital. The band dispersion relation completely describes the electronic properties of the chain for energies above the Fermi level. $E_n(k)$ points obtained for shorter chain lengths follow a parabolic dispersion with similar effective mass but a reduced density of points per energy interval. The effective mass of $0.5m_e$

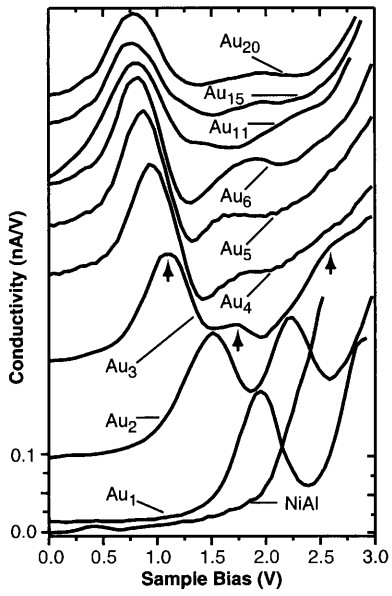

Fig. 2. Conductivity spectra for bare NiAl and for Au chains with different lengths. Spectra were taken in the center of the chains and are offset for clarity. The tunneling gap was set at V_{sample} = 2.5 V, I = 1 nA. Electronic resonances of Au_3 are marked with arrows.

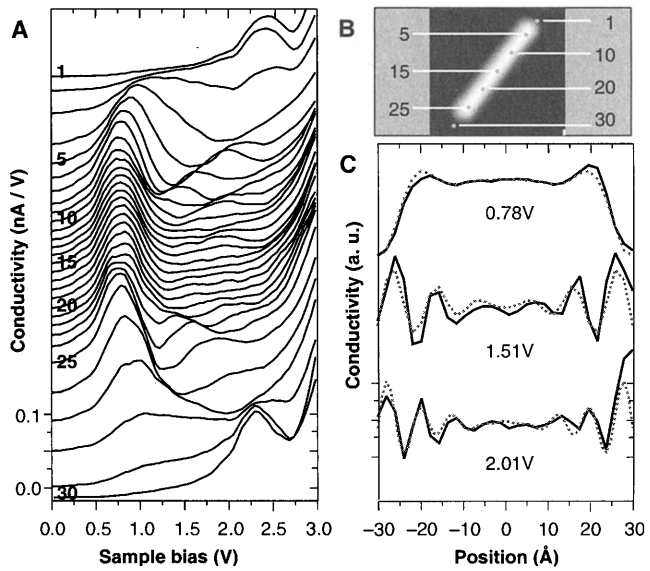

Fig. 3. (**A**) Conductivity spectra taken along Au_{20} with a tunneling gap set at V_{sample} = 2.5 V, I = 1 nA. (**B**) The positions are marked in the topographic image of Au_{20}. (**C**) Vertical cuts through *dI/dV* spectra shown in (A) at three exemplary energies. Conductivity patterns are fitted with the sum of squared sinusoids of fixed wave vector, $\pi n/L$, and adjustable weight c_n (dotted curves). The derived coefficients are c_1 = 0.31, c_2 = 0.29, c_3 = 0.26, c_4 = 0.11 for 0.78 V; c_5 = 0.26, c_6 = 0.50, c_7 = 0.24 for 1.51 V; and c_6 = 0.13, c_7 = 0.29, c_8 = 0.39, c_9 = 0.19 for 2.01 V.

for Au chains on NiAl(110) lies between the values for the bulk Au sp-band [$1.1m_e$ (*19*)] and the Au(111) surface state [$0.25m_e$ (*21*)]. On a stepped Au(788) surface, a 1D state with $0.27m_e$ was identified by photoelectron spectroscopy (*12*). Gold chains formed on Si(111) are characterized by a filled electron band with $0.5m_e$ (*22*). The actual value of the effective mass depends on the coupling between neighboring Au atoms. However, experiments on low-dimensional metal structures correspondingly observe effective masses smaller than in the bulk material, indicating higher electron mobility in reduced dimensionality.

The dispersion relation obtained for the empty electron band in a Au_{20} chain can be used to test further predictions for a 1D electron gas. The energy of the first quantum well state ($n = 1$) scales with the square of the corresponding wave vector $k^2 = (\pi n/L)^2$, according to Eq. 1. The resulting L^{-2} dependence on the chain length was fitted to the energy position of the lowest *dI/dV* resonance for Au chains with an increasing number of atoms (Fig. 4C). Except for the monomer, where the concept of a 1D electron gas certainly breaks down, the measured peak positions follow the expected L^{-2} dependence. The measured energy dependence of the DOS in Au chains can also be compared with the idealized 1D behavior, which is characterized by a sharp onset and a $E^{-1/2}$ decay with increasing energy (*19*). The relative DOS for a Au_{20} chain (Fig. 4D) is obtained by averaging *dI/dV* spectra from Fig. 3A and subtracting an exponentially increasing function to account for the conductivity of the bare NiAl. The result reflects qualitatively the predictions of the $E^{-1/2}$ dependence; the *dI/dV* intensity is maximal at the band onset of 0.68 eV and decreases rapidly for higher energies. Variations from the perfect 1D behavior are attributed to the finite length of the chain and the limited number of states on the parabolic band. For a 60 Å quantum well, the positions of the energy levels are determined by Eq. 1 (Fig. 4D, bars on the left). A broadening of these levels with the experimental line width of 0.35 eV yields an energy dependence of the DOS, which is in reasonable agreement with the *dI/dV* behavior measured for a Au_{20} chain.

The two ends of Au chains on NiAl(110) introduce a break of translational symmetry in the 1D electronic structure. In analogy to the formation of 2D defect states at the surface of a bulk crystal, the appearance of a zero-dimensional state is expected for linear structures (*23*). A pronounced *dI/dV* peak around 2.4 V was indeed detected for tip positions slightly outside the Au_{20} chain (Fig. 3A) and was also observed for shorter chain lengths (Fig. 4C). Because of the weak length dependence and a localization outside the chains, these *dI/dV* resonances are attributed to zero-dimensional defect states formed at the ends of a 1D quantum well.

The 1D particle in the box model certainly oversimplifies the electronic properties in Au chains. The adsorption of Au atoms on a NiAl(110) surface leads to a hybridization of Au orbitals with substrate electronic states. The interaction between single Au atoms in the 1D chains therefore results from a direct overlap between the Au wave functions and substrate-mediated mechanisms, such as adsorbate-induced Friedel oscillations in surface states (*9*, *24*). Experiments on Au pairs with variable interatomic separation will provide further insights into the interaction mechanisms on the NiAl(110) surface. The strong electron-phonon coupling occurring in 1D systems is known to change the periodicity along atomic chains in a Peierls distortion (*25*). The driving force behind the transition is an opening of band gaps at the Fermi level due to the creation of a new Brillouin zone in reciprocal space. No changes in the atom periodicity could be detected for Au chains on NiAl(110). Because the observed electron band is localized above the Fermi level, small deviations cannot modify the electron occupation of the band and are ineffective in reducing the total energy of the Au chains. Peierls distortions may, however, be present for different material combinations, where the adsorbate-induced electron band crosses the Fermi level of the system.

The experiments described here demonstrate an approach to studying the correlation between geometric and electronic properties of well-defined 1D structures. The investigation of 2- and even 3D objects, built from single atoms, is envisioned. Because STM is also sensitive to vibrational, optical, and magnetic properties, the unique behavior of matter in the atom-to-bulk transition range can be profoundly analyzed in artificial nanostructures, opening the way for various potential applications in electronic, chemical, optical, and magnetic technologies.

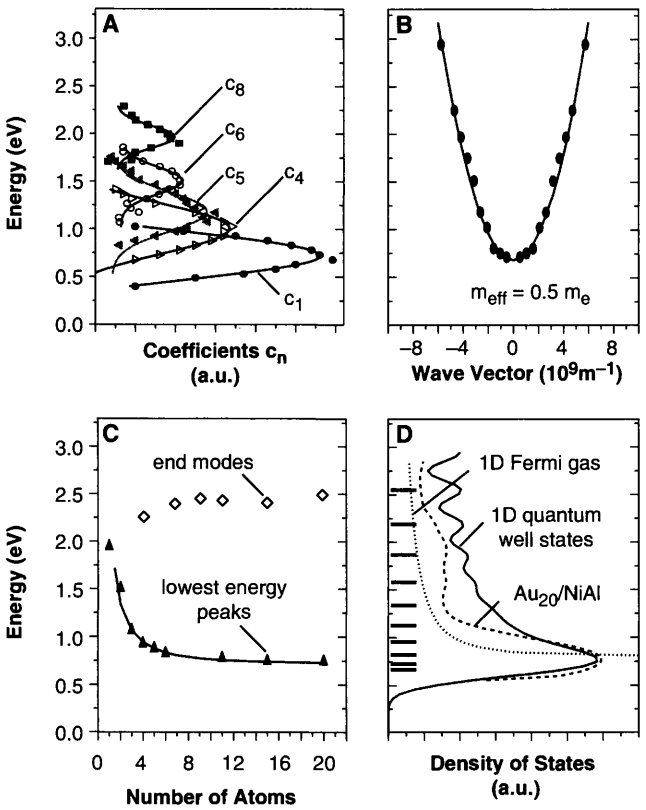

Fig. 4. (**A**) Selected coefficients c_n obtained from the fitting procedure of conductivity patterns along a Au_{20} chain. The maximum for each c_n identifies the energy of the eigenstate with wave vector $k = \pi n/L$. (**B**) Dispersion relation of electronic states for a Au_{20} chain, with each point (E,k) obtained from (**A**). (**C**) Lowest energy conductivity peaks and end modes for Au chains with an increasing number of atoms. The lowest energy peaks for Au_3-Au_{20} are fitted with an L^{-2} dependence on chain length L (solid lines). (**D**) Energy dependence of the conductivity for a Au_{20} chain (dashed line) in comparison to the calculated DOS for a 60 Å long quantum well (solid line) and a 1D free-electron gas (dotted line). Quantum well states are marked with bars along the left axis.

References and Notes

1. G. Ertl, H. Knözinger, J. Weitkamp, Eds., *Handbook of Heterogeneous Catalysis* (Wiley-VCH, Weinheim, Germany, 1997).
2. M. Valden, X. Lai, D. W. Goodman, *Science* **281**, 1647 (1998).
3. U. Kreibig, W. Vollmer, *Optical Properties of Metal Clusters* (Springer Series in Materials Science, Springer, Berlin, 1995), vol. 25.
4. N. Nilius, N. Ernst, H.-J. Freund, *Phys. Rev. Lett.* **84**, 3994 (2000).
5. H. Haberland, Ed., *Clusters of Atoms and Molecules* (Springer, Berlin, 1993).
6. C. Binns, *Surf. Sci. Rep.* **44**, 1 (2001).
7. S. D. Kevan, R. H. Gaylord, *Phys. Rev. B* **36**, 5809 (1987).
8. J. Kliewer *et al.*, *Science* **288**, 1399 (2000).
9. J. Repp *et al.*, *Phys. Rev. Lett.* **85**, 2981 (2000).
10. W. Widdra *et al.*, *Phys. Rev. Lett.* **80**, 4269 (1998).
11. P. Segovia, D. Purdie, M. Hengsberger, Y. Baer, *Nature* **402**, 504 (1999).
12. A. Mugarza *et al.*, *Phys. Rev. Lett.* **87**, 107601 (2001).
13. M. Bockrath *et al.*, *Nature* **397**, 598 (1999).
14. M. F. Crommie, C. P. Lutz, D. M. Eigler, *Nature* **363**, 524 (1993).
15. B. C. Stipe, M. A. Rezaei, W. Ho, *Rev. Sci. Instrum.* **70**, 137 (1999).
16. L. Bartels, G. Meyer, K. H. Rieder, *Phys. Rev. Lett.* **79**, 697 (1997).
17. Absolute peak positions deviate by ±0.1 V for dif-

ferent tips, most likely due to changes in tip-induced electric field.
18. S. C. Lui, M. H. Kang, E. J. Mele, E. W. Plummer, D. M. Zehner, *Phys. Rev. B* **39**, 13149 (1989).
19. C. Kittel, *Introduction to Solid State Physics* (Wiley, New York, 1996).
20. The *dI/dV* signal is proportional to the DOS $\rho(E)$ in the quantum well with $\rho(E) = \Sigma c_n |\phi_n(k)|^2$. The corresponding energy levels $E_n(k)$ are eigenstates of the Schroedinger equation for wave functions $\phi_n(k)$. Wave functions in a 1D quantum well have the form $\phi_n(k) = {}^1/_2\sin(kx)$ with $k = \pi n/L$. To determine the coefficients c_n, $\rho(E)$ is fitted to the observed *dI/dV* pattern.
21. S. LaShell, B. A. McDougall, E. Jensen, *Phys. Rev. Lett.* **77**, 3419 (1996).
22. K. N. Altmann *et al.*, *Phys. Rev. B* **64**, 035406 (2001).
23. E. Bertels, *Surf. Sci.* **331**, 1136 (1995).
24. A. Bogicevic *et al.*, *Phys. Rev. Lett.* **85**, 1910 (2000).
25. K. Swamy *et al.*, *Surf. Sci.* **482**, 402 (2001).
26. This material is based on work supported by the National Science Foundation under grant 0102887. The award of a fellowship to N.N. by the Deutsche Forschungsgemeinschaft is gratefully acknowledged. We are greatly indebted to M. Persson for stimulating discussions and illuminating calculations. Additional insights have been provided by R. B. Muniz, D. L. Mills, and R. Wu.

19 June 2002; accepted 6 August 2002
Published online 22 August 2002;
10.1126/science.1075242
Include this information when citing this paper.

A Major Archean, Gold- and Crust-Forming Event in the Kaapvaal Craton, South Africa

Jason Kirk,[1]* Joaquin Ruiz,[1] John Chesley,[1] John Walshe,[2] Gavin England[3]

The 2.89- to 2.76-gigayear-old conglomerates of the Central Rand Group of South Africa host an immense concentration of gold. The gold and rounded pyrites from the conglomerates yield a rhenium-osmium isochron age of 3.03 ± 0.02 gigayears and an initial $^{187}Os/^{188}Os$ ratio of 0.1079 ± 0.0001. This age is older than that of the conglomerates. Thus, the gold is detrital and was not deposited by later hydrothermal fluids. This Middle Archean gold mineralization event corresponds to a period of rapid crustal growth in which much of the Kaapvaal craton was formed and is evidence for a significant noble metal flux from the mantle.

South Africa's Witwatersrand Supergroup (WSG) gold deposits have produced over 48,000 metric tons of gold and have accounted for about 40% of the world's total historic production (*1*). Attempts to date WSG gold mineralization remain equivocal, yielding a complex geochronology with ages that reflect multiple disturbances (*2–9*). Here, we determine the age of the gold mineralization to improve our understanding of the processes responsible for the changing styles and magnitudes of gold deposition.

The WSG, located in the Kaapvaal craton of South Africa (fig. S1), composes an ~7-km-thick sequence of detrital terriginous sediments (*2*, *10*) derived from the erosion of older granite-greenstone belts in fluvial deltaic settings (*11*). The WSG is divided into a lower West Rand Group and an upper Central Rand Group (CRG), with gold production largely confined to the quartz pebble conglomerates of the CRG (*1*). A maximum age for deposition of the CRG of 2.89 gigayears ago (Ga) has been obtained from the youngest detrital zircons found in the lower CRG (*12*), and a minimum age of 2.76 Ga was determined based on the oldest authigenic xenotime Pb ages in the CRG (*9*).

Geochronology of the WSG provenance includes U-Pb ages on detrital zircons and monazites, which yield an age range from 3.3 to 2.8 Ga (fig. S1). U-Pb and Pb-Pb isotopic ages from rounded uraninite (*3*) and pyrite grains (*4*), as well as Os isotopic model ages from osmiridium grains (*5*) and gold grains (*6*), are all between about 3.5 and 2.9 Ga, and thus these phases have been interpreted as being of detrital origin (fig. S1). U-Pb and Pb-Pb ages on pyrites, uraninites, hydrothermal zircon, rutile, and xenotime, as well as K-Ar ages on clays and micas, are between about 2.7 and 2.0 Ga (*1*, *2*, *7*, *9*). These younger ages have been used to define a series of at least five tectonothermal events that may have introduced and/or mobilized gold (fig. S1).

The superimposed metamorphism on the conglomerate hosts of the WSG has led to contentious debate on the age and origin of gold, centered around placer and epigenetic models. In placer models, gold and associated rounded pyrite are detritus from unidentified

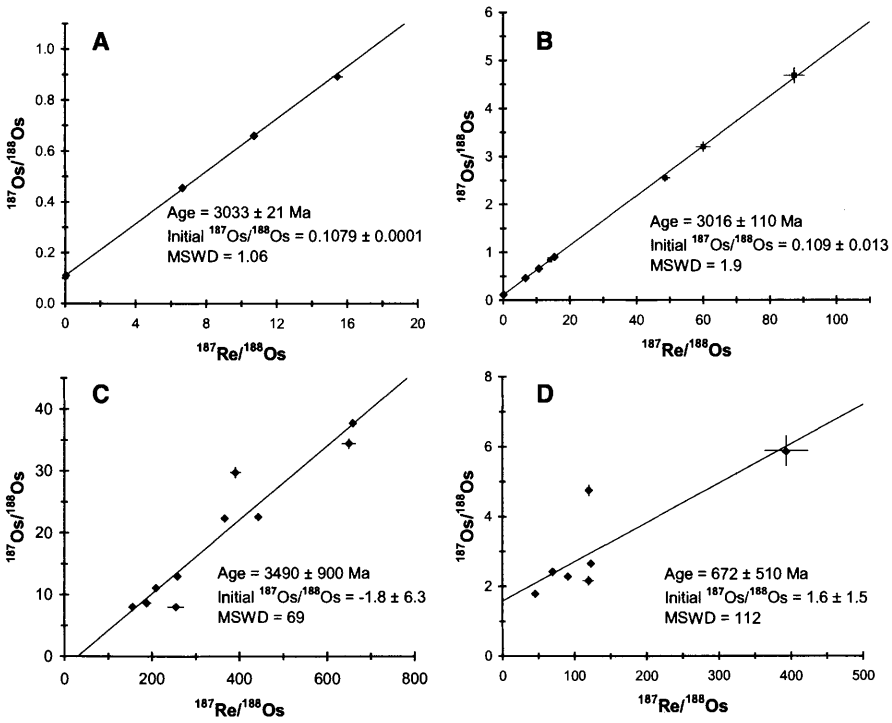

Fig. 1. Re-Os isochron diagrams for WSG samples. In all isochrons, errors are represented by crosses or are smaller than the symbols used. Errors were determined by using the greater of either the 2σ counting error ($2SD\sqrt{n}$) or by varying the Os blank between measured values of 1 to 2 pg. All isochrons were calculated using Isoplot (*25*). (**A**) VR gold samples. (**B**) VR gold and rounded VR pyrites. Filled squares represent pyrite samples; filled diamonds represent gold samples. (**C**) SR rounded pyrite samples. (**D**) VCR euhedral pyrites.

[1]Department of Geosciences, University of Arizona, Tucson, AZ 85721, USA. [2]Commonwealth Scientific and Industrial Research Organisation, Division of Exploration and Mining, 39 Fairway, Nedlands 6009, Western Australia. [3]Geology and Geophysics Department, University of Edinburgh, Edinburgh EH9 3JW UK.

*To whom correspondence should be addressed. E-mail: jkirk@geo.arizona.edu